

Shape Effects on Microbody Impacts against a Flat Surface

W. Cheng, R. M. Brach, and P. F. Dunn

*Particle Dynamics Laboratory, Department of Aerospace and Mechanical Engineering,
University of Notre Dame, Notre Dame, Indiana*

A general numerical model is developed to simulate the impact of an elongated microbody with a spherical tip against a flat surface. Experimental data of sphere impacts are used to determine the parameters used in the simulations. Two kinds of microbodies are considered: a rod with spherical ends and 2 hemispheres connected by a thin rigid rod. The results show that under the same incident velocity and orientation angle, the impacts are affected by the microbody shape. Angular velocity changes are quite sensitive to the length and orientation of the rod. Rotational energy balance plays an important role for long microbodies. The rebound velocity at the contact tip and the center of mass is different and can lead to secondary impacts. In contrast to spheres, tangential (friction) and normal forces are coupled for elongated microbodies. Because the tangential and normal forces act over the contact area at the end of the rod, a moment about the mass center is produced. The rotation of the rod is driven by this moment, which, in turn, changes the relative velocity and contact forces over the contact area. Thus the coefficient of restitution at the contact tip is also effected by and becomes a function of the geometry and orientation of the microbody. The simulation results support that three-dimensional (3D) microbody impact response is determined not only by the material and incident velocities but also by the geometry and orientation of the principal axis of the microbody.

INTRODUCTION

Microbody deposition onto surfaces occurs in many applications, such as filtration, surface coating, and contaminant detection. In this paper, only smooth, flat surfaces are considered. Usually, to simplify the problem, microbodies are treated as microspheres. Most studies separate the contact process and forces into normal and tangential components (Israelachvili and

Tabor 1972). The theoretical contact area of spherical surfaces in Hertzian contact with adhesion has been calculated by Johnson et al. (1971) and Derjaguin et al. (1975). Concerned about the normal and tangential loading, Skinner and Gane (1972) and Ando et al. (1995) measured the friction and the normal attraction forces between surfaces under micro-loads. Several impact models have been developed based on these works to predict the rebound velocity of the microsphere (Dahneke 1975; Wall et al. 1990; Tsai et al. 1991; Xu and Willeke 1993; Brach and Dunn 1995). Experiments and numerical simulations have focused on the prediction of the rebound velocities for normal impact or oblique impact of spheres (Li et al. 1999). However, no angular velocity data was published because accurate measurements of microbody rotation, and sliding during impact could not be made. Numerical simulation offers an alternative and important way to understand the effects of incident angle, rotation, and initial velocities on microbody impact. A more obvious reason to do numerical simulation is that without simulation one can never fully understand the response of such a highly nonlinear dynamic model under complicated circumstances. A three-dimensional (3D) model for microsphere impacts has been introduced by Cheng et al. (2002). In that paper, numerical results are generated and analyzed for complicated initial conditions.

The effects of microbody geometry cannot be considered using sphere impact simulations. In reality, the shape of the microbody can also be important in the mechanics of impact. In order to identify the significance of the geometry of the microbody, a 3D simulation model for an arbitrarily-shaped microbody impacting a flat surface is developed in this paper. The model is compared to the simulation of sphere impacts. Then the impacts of a rod with spherical ends and also 2 hemispheres connected by a thin rigid rod are used to investigate the effects of initial conditions and geometrical parameters.

CONTACT MODEL

A model for the impact of an arbitrarily-shaped microbody with a smooth flat surface is developed in order to investigate the effects of the shape of the microbody on the behavior of the

Received 1 August 2001; accepted 14 March 2002.

This research was supported by the Center for Indoor Air Research (contract no. 96-06) and the Electric Power Research Institute (contract no. RP 8034-03).

Address correspondence to Patrick F. Dunn, 107 Hessert Center, Notre Dame, IN 46556. E-mail: patrick.f.dunn.1@nd.edu

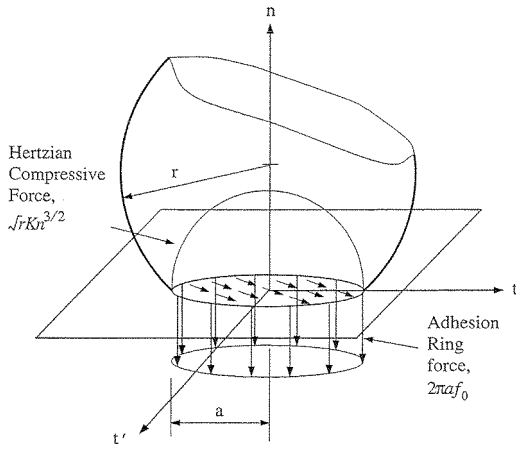


Figure 1. A schematic of the spherical end of a microbody in contact with a flat surface.

impact. The contact region of the microbody and surface is still considered to be spherical and Hertzian elastic theory and the adhesion ring force model used in the sphere impact simulation by Brach and Dunn (1995) is assumed to remain valid. In the current simulation, the kinetic energy is assumed to be dissipated only in the contact region (the spherical tip). No plastic or internal energy dissipation is considered. The local spherical contact region is modeled with Brach and Dunn's simulation model (1995) using a ring-force model for adhesion loading. Because the deformation and the contact area are small compared to the local curvature radius of the spherical tip and the size of the microbody, the microbody is considered to be an infinite half-space in the evaluation of contact forces and a rigid body in the kinematic computation. Figure 1 shows the local geometry and coordinate system of the hemispherical contact tip. Typically the contact radius, a , is small compared to the curvature radius, r . Because the microbody is small and the impact durations are short, the effects of gravity are negligible. Material and adhesion dissipation are nonlinear but are assumed to be dependent on the first power of the normal velocity. Mathematical analysis shows that higher power velocity dependent dissipation, under most circumstances, does not make a significant difference compared to the first power approximation.

According to Brach and Dunn's simulation model, during contact the normal contact force for the microbody is

$$F_n = \sqrt{rK}(-n)^{3/2}(1 - C_H \dot{n}) - 2\pi a f_0(1 + C_A \dot{n}). \quad [1]$$

The first term of the right side of Equation (1) is the Hertzian force and the corresponding material damping. Without the second term, this equation describes pure Hertzian elastic contact. However, the second term, the adhesion and damping force, makes the contact adhesive. The adhesion force is modeled by a ring force acting on the periphery of the circular contact area. The current adhesive contact model can be related to the Johnson-Kendall-Roberts (JKR) theory (Johnson et al. 1971). At the equi-

librium position, in which the velocity and the resultant normal force is zero, both the JKR model and the current model produce the same equilibrium contact radius. This condition gives the relationship between the adhesion line force, f_0 , and other material parameters (Li et al. 1999):

$$f_0 = \left(\frac{9}{2\pi} K r w_A^2 \right)^{1/3}. \quad [2]$$

However, Equation (1) does not predict the so-called snap-off and snap-on procedure. In Equation (1) the Hertzian elastic force and the adhesion force are all zero when there is no normal displacement ($n = 0$). The adhesion force and the contact area appear only when there is normal displacement. In other words, once the contact area is formed, the sphere tip will be deformed and this will give a normal displacement, n . However, the JKR theory produces the contact area and the adhesion force first and this initial "snap-on" does not cause any normal displacement. The parameters in Equations (1) and (2) are the material stiffness, K , the combined surface energy, w_A , and damping coefficients, C_H and C_A , for Hertzian and adhesion damping, respectively. The adhesion line force, f_0 , can be calculated from Equation (2). The relative displacement of the mass center is n where $n \leq 0$ during contact and $n < 0$ initially. The original radius of the spherical end is r , and a is the contact radius. As predicted by Hertzian theory,

$$a = \sqrt{-rn}, \quad n \leq 0. \quad [3]$$

Through dimensional analysis, the damping constants can be put into a nondimensional form:

$$C_H = \zeta_H \left(\frac{4\pi^8}{5} \right)^{3/2} v_0^{-1/4} (f_0^3 K^{5/2} r^{-3} \rho^{-1})^{-3/4}, \quad [4]$$

$$C_A = \zeta_A \left(\frac{3\pi^8}{5} \right)^{3/5} v_0^{-1/4} (f_0^{-4/5} K^{9/10} r^{2/5} \rho^{-1/2})^{-3/4}, \quad [5]$$

where ζ_A and ζ_H are the nondimensional Hertzian and adhesion damping parameters that are determined through the experimental data of normal impact. The velocity, v_0 , is a positive reference velocity, which is the normal incident velocity in the simulation. A form of Coulomb friction with a coefficient f is used to model the tangential forces:

$$F_t = -f |F_n| \cos \psi, \quad [6]$$

$$F_{t'} = -f |F_n| \sin \psi, \quad [7]$$

where ψ is the directional angle of the relative tangential velocity on the contact surface. F_n is the resultant normal force over the contact area, which is equal to the right-hand side of Equation (1).

Coulomb friction is nonlinear in this model. The nonlinearity is caused by the absolute value of F_n in Equations (6) and (7). At the beginning and the end stage of contact, the normal force

Table 1
The basic parameters for numerical simulation
(Wall et al. 1990)

r_0 (μm)	Density		w_A (J/m^2)	f	ζ_A	ζ_H
	(kg/m^3)	K ($\times 10^9$ Pa)				
2.45	1350	0.174	0.38	0.15	0.5	1.5

is negative due to the fact that for small displacement, n , the adhesion force is larger than the Hertzian elastic force. Thus friction for a “pulling” force contact has to be modeled. In the current simulation model, the tangential friction force is assumed to be proportional to the magnitude of the total normal force, including the adhesion attraction process. Friction exists due to the relative tangential motion at the interface. The problem of friction under negative normal load has not been fully resolved. There are some measurement results by Skinner and Gane (1972) that show the same relationship between friction and negative normal loading as used here. Values of the material parameters used in the simulation are listed in Table 1.

RIGID BODY KINEMATICS

The deformation on the contact tip predicted by Brach and Dunn’s model is small compared to the geometry of the microbody. Thus the motion of the whole microbody is modeled by rigid body kinematics. The initial angles of the microbody’s principal axes with substrate surface are given as initial conditions and the principal moments of inertia are treated as known parameters in the simulation. Consider the arbitrarily-shaped microbody A shown in Figure 2. Let \bar{n}_1^A , \bar{n}_2^A , and \bar{n}_3^A represent a set of dextral orthogonal unit vectors attached to the rigid body A , and let \bar{n}_1 , \bar{n}_2 , and \bar{n}_3 be the dextral orthogonal unit vectors representing an inertia reference frame R (in this case moving

with the translation of the center of mass), as shown in Figure 2. The rotating frame fixed to a rigid body can be related to the inertial frame, R , by 3 successive rotations. If the 3 successive rotations are denoted by α , β , and γ , a matrix, S , called the *direction cosine matrix* can be defined, which relates the base unit vectors, \bar{n}_i , to the body unit vectors, \bar{n}_i^A ($i = 1, 2, 3$). In matrix form, the relation is

$$\bar{n}^A = S\bar{n}, \quad [8]$$

where \bar{n}^A is the unit vector for the rotating frame and \bar{n} is the unit vector for the translation inertia frame fixed on the mass center.

Consider a vector, \bar{r} , fixed on a rigid body, A , as shown in Figure 2. Define

$$\frac{d\bar{r}^A}{dt} = {}^R\bar{\omega}^A \times \bar{r}, \quad [9]$$

where ${}^R\bar{\omega}^A$ is viewed as an operator that produces the total derivatives of \bar{r} by cross multiplication. The components of the angular velocity are given by a skew matrix, Ω , such that

$$\Omega = \mathcal{S}S^T, \quad [10]$$

$$\Omega_{ij} = \varepsilon_{jin}\omega_n = \begin{pmatrix} 0 & -\omega_3 & \omega_2 \\ \omega_3 & 0 & -\omega_1 \\ -\omega_2 & \omega_1 & 0 \end{pmatrix}, \quad [11]$$

and the angular velocity vector is

$$\bar{\omega} = \omega_1\bar{n}_1 + \omega_2\bar{n}_2 + \omega_3\bar{n}_3. \quad [12]$$

In matrix form, the transform from rotations α , β , and γ is

$$\begin{pmatrix} \omega_1 \\ \omega_2 \\ \omega_3 \end{pmatrix} = T \begin{pmatrix} \alpha \\ \beta \\ \gamma \end{pmatrix}, \quad [13]$$

where

$$T = \begin{pmatrix} \cos \beta \cos \gamma & \sin \gamma & 0 \\ -\cos \beta \sin \gamma & \cos \gamma & 0 \\ \sin \beta & 0 & 1 \end{pmatrix}. \quad [14]$$

Thus the rates of Euler angles in the expressions of angular velocities are

$$\begin{pmatrix} \dot{\alpha} \\ \dot{\beta} \\ \dot{\gamma} \end{pmatrix} = T^{-1} \begin{pmatrix} \omega_1 \\ \omega_2 \\ \omega_3 \end{pmatrix} \quad [15]$$

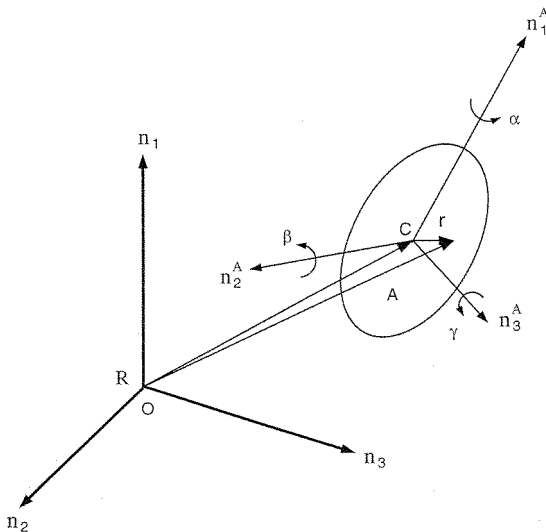


Figure 2. The rotating frame A and the translating frame R .

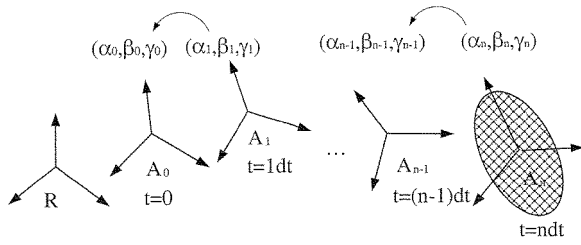


Figure 3. A set of unit vectors fixed in the rigid body A and defined with respect to a set of auxiliary frames. The numerical time increment is represented by dt .

Because of the arbitrary shape of the microbody, the orientation of the principle axes changes during impact. This causes difficulty for numerical simulation. In order to trace the microbody position in each time step, a set of intermediate reference frames and the corresponding transforms are used. By computation of the Euler angles, the position of the microbody is adjusted according to the rotation and translation of the microbody. Figure 3 shows a set of unit vectors fixed in the rigid body A and defined with respect to a set of auxiliary frames that is used in the calculation. The computational loop of the simulation begins with the initial frame, A_0 . The initial Euler angles of the principle axis $(\alpha_0, \beta_0, \gamma_0)$ are offered as initial conditions. The initial direction cosine matrix is $S_R^{A_0} = S(\alpha_0, \beta_0, \gamma_0)$. It is easy to show that the inverse transform is $S_R^{A_0} = S_R^{A_0^{-1}} = S_R^{A_0^T}$. The procedure is as follows.

1. Calculate $S_R^{A_0} = S(\alpha_0, \beta_0, \gamma_0)$ and $S_{A_0}^R = S_{A_0}^{A_0^T}$.
2. Transform the force and moment vectors from frame R to frame A :

$$\begin{cases} \bar{F}^{A_0} = \bar{F}^R S_{A_0}^R, \\ \bar{M}^{A_0} = \bar{M}^R S_{A_0}^R. \end{cases} \quad [16]$$

3. Integrate the following Ordinary Differential Equation (ODE) by the fourth-order Runge-Kutta-Gill (R-K-G) method to get the angular velocities ω_i :

$$\omega_{ij} I_j = \varepsilon_{ijk} r_j^A F_k^A + M_i^A, \quad [17]$$

where I_j ($j = 1, 2, 3$) is the moment of inertia about the principle axis of the microbody, r_j is the moment arm vector of the total contact force, \bar{F}^A , and

$$\omega_{ij} = \begin{pmatrix} \omega_1 & 0 & 0 \\ 0 & \omega_2 & 0 \\ 0 & 0 & \omega_3 \end{pmatrix}. \quad [18]$$

4. According to the relationship shown by Equation (15), find the rate of Euler angles $(\dot{\alpha}, \dot{\beta}, \dot{\gamma})$. Solve Equation (15) by fourth-order R-K-G method, and find the variation of Euler angles in one time step $(d\alpha, d\beta, d\gamma)$. Calculate the

corresponding transform matrix, $S_{A_0}^{A_1} = S(d\alpha, d\beta, d\gamma)$ and $S_R^{A_1} = S_R^{A_0} S_{A_0}^{A_1} = S(\alpha_0, \beta_0, \gamma_0) S(d\alpha, d\beta, d\gamma)$.

5. Evaluate the contact forces and contact moments for the new time step (the frame A_1). Find \bar{F}^R and \bar{M}^R , then transform them into the frame A_1 by

$$S_{A_1}^R = S_{A_1}^{A_1^T} \quad [19]$$

and

$$\begin{cases} \bar{F}^{A_1} = \bar{F}^R S_{A_1}^R, \\ \bar{M}^{A_1} = \bar{M}^R S_{A_1}^R. \end{cases} \quad [20]$$

6. Repeat steps 2 through 5 until the end of the impact. When the normal displacement returns to zero and the normal velocity is positive, the impact is ended.

In Figure 4, O' is the center of the spherical contact region of the microbody. O is the center of the contact area, and C is the mass center of the microbody. The vector \bar{r}_0 is the position vector of the center of the spherical tip, $\bar{O}'O$, and \bar{d} is the position vector of the mass center, $\bar{C}O'$. \bar{r}_0 is always upward in frame R :

$$\bar{r}_0^R = -r_0 \bar{n}_1. \quad [21]$$

\bar{d} is always along the $-\bar{n}_1^{A_i}$ direction, where A_i is the reference frame in time step i ($i = 0, 1, \dots, N$):

$$\bar{d}^{A_i} = -d \bar{n}_1^{A_i}, \quad [22]$$

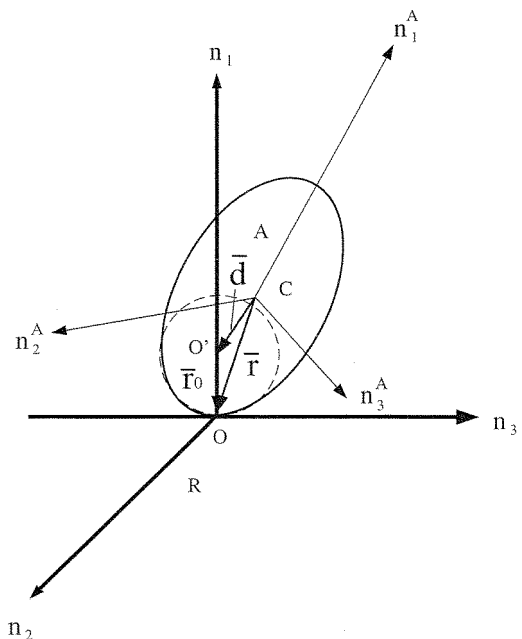


Figure 4. The schematic of a microbody on a flat surface.

so the position vector \bar{r} of the mass center in frame R , \bar{r}^R is

$$\bar{r}^R = d^R + \bar{r}^R = (-dS_{Ai}^R - r_0) \bar{n}_1. \quad [23]$$

The contact forces are computed based on the relative velocity between the microbody and the surface over the contact area in the frame R at time step i , which can be derived by the following equations:

$$\bar{v}_r^R = {}^R\bar{\omega}^{Ai} \times \bar{r}^R + \bar{v}_c, \quad [24]$$

where \bar{v}_c is the translational velocity of the mass center and ${}^R\bar{\omega}^{Ai}$ is the rigid body angular velocity in frame R at time step i :

$${}^R\bar{\omega}_i^{Ai} = S_{Ai}^R \bar{\omega}_i^{Ai}. \quad [25]$$

There are 2 stages in the normal microbody impact: approach and rebound, separated by an instant of zero relative normal velocity of point O' . The impact starts with a zero normal displacement and a negative normal velocity (toward the surface). When the relative normal contact velocity is negative, $v_{r1} < 0$, the motion of the microbody is toward the surface. The impact is in the approach stage. Because of the contact interaction forces between the microbody and the surface, the normal velocity in the contact region decreases. At the end of approach, the velocity of the microbody at O' becomes zero and the contact area is positive. During rebound, the normal contact velocity becomes positive, $v_{r1} > 0$. Equations of motion introduced previously are integrated by the R-K-G method with initial conditions of $n(0) = 0$ and $\dot{n}(0) = v_{r1}(0)$. The whole process stops until the normal contact displacement of the microbody becomes zero again, which means that $n = 0$ and $\dot{n} > 0$. If there is any tangential relative velocity in the contact area, v_{r2} or v_{r3} equals to zero, then a pure rolling contact or velocity reversal occurs. The critical friction force, F_c^R , necessary to keep the microbody from sliding is calculated. If $F_c^R \leq \mu F_n$, then the microbody will return to sliding, otherwise the microbody will remain the pure rolling condition. If neither of the tangential contact velocity components is zero, then Coulomb friction is calculated according to the following equation:

$$F_i^R = -f\xi F_n \text{sgn}(v_{ri}), \quad (i = 2, 3), \quad [26]$$

where f is the Coulomb friction coefficient and ξ is the *direction cosine* of the contact velocity projection on the \bar{n}_i direction.

NUMERICAL SIMULATION RESULTS

Three types of body geometries are used in the numerical simulation for different purposes. A sphere is used to identify potential errors in the arbitrarily-shaped body impact model and to validate the model to the extent possible through the 2D case of sphere impact. A structure consisting of 2 hemispheres connected by a thin rigid rod with no mass is used to identify the effects of the length of the microbody on impact. Finally, a rod with hemispherical ends (see Figure 6) is used to investigate

the combined effects of the initial orientation, geometry, and mass on the impact results. At the present stage, because of the difficulties in experimental measurements of the microrotation and tangential motion in a short time period (nanoseconds), no data are available for the verification of the simulation results for a microbody with a geometry other than spherical. Even for spheres, rotational effects must be inferred. The practical meaning of the simulation is to reveal the possible significance of the shape of the microbody on the impact results and some new characteristics generated by the aspects of the geometry. For example, the results show that the coefficient of restitution at the contact tip for a given initial condition and fixed material properties is not a constant. It is also a function of the geometric shape and initial orientation of the microbody. The possibility of a secondary impact and the capture condition for an arbitrarily-shaped microbody are related to its geometry and initial conditions (including orientation). These results may be interesting for future experimental measurements.

Sphere

A sphere can be seen as a rod with hemispherical ends and zero length (represented by L in Figures 5 and 6). Because of symmetry, sphere impacts are not affected by the transform of coordinate systems and the Euler angles of the principle axis. Sphere impacts are simulated using both the 3D arbitrarily-shaped body model and the sphere model (Cheng et al. 2002) in parallel and the results are compared. The comparison shows the independence of Euler angles and the agreement of the results between these 2 models. The simulation results for sphere impact are also compared to the experimental data by Wall et al. (1990). Figure 7 shows one example of these simulation results. In the figure, parameters with values listed in Table 1 are fixed for 4 different sphere diameters. The simulation results predict very well the coefficients of restitution for different diameter and different incident velocities. The simulations are verified at least for the 2D sphere impact. In order to describe and compare the simulation results, 2 restitution coefficients are defined. The restitution coefficient, e_n , is the ratio of the magnitude of rebound

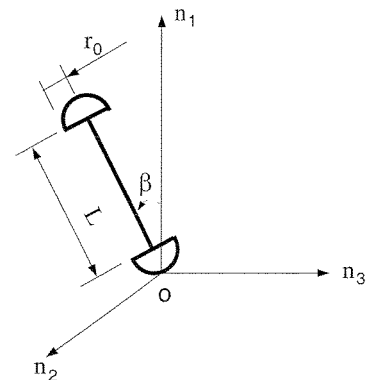


Figure 5. The schematic of 2 hemispheres connected by a rigid bar with no mass and the incident angle ($\alpha = \gamma = 0^\circ$).

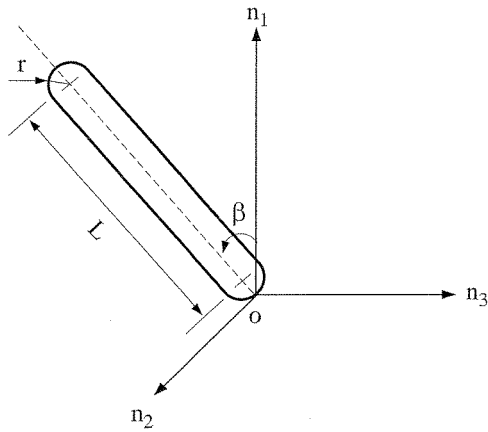


Figure 6. The schematic of the rod and the incident angle ($\alpha = \gamma = 0^\circ$).

(subscript, r) to initial (subscript, i) normal (subscript, n) velocity at the contact tip (subscript, c):

$$e_n = \frac{v_{cr_n}}{v_{ci_n}} \quad [27]$$

The restitution coefficient, e_{nm} , is the ratio of the magnitude of rebound to initial normal velocity at the center of mass (subscript, m):

$$e_{nm} = \frac{v_{mr_n}}{v_{mi_n}} \quad [28]$$

For all numerical results, the integration interval was chosen to be small enough to yield consistent results, but not to cause significant round-off errors. The tolerance level was set such that the global difference in solutions ranged from <1 part in 10^7 to <1 part in 10^{10} .

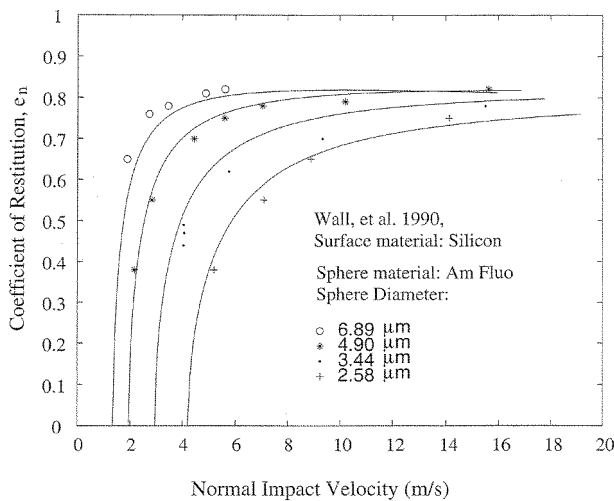


Figure 7. Simulation results versus experimental data for 2D sphere impacts.

Massless Rod and Hemispheres

The microbody geometry in Figure 5 is used in the simulation. The microbody is 2 hemispheres connected by a rigid-body bar with no mass. The radius of the hemisphere is r_0 and the length of the rigid bar is L . The shape of the microbody is described by the length ratio, $\rho_r = L/r_0$. Figure 5 also shows the definition of orientation angle, which is the angle β , with $\alpha = \gamma = 0^\circ$. The microbody shown in Figure 5 is suitable to investigate the effects of the length ratio on the impact results because for a given radius, r_0 , and fixed material properties, the mass and the damping of the impact according to Equations (4) and (5) do not change when the length ratio changes. Therefore the impact results are affected purely by the length ratio ρ_r .

To analyze the simulation results, 2 coefficients of restitution are defined: the coefficient of restitution at the contact tip, e_n , and the coefficient of restitution at the mass center, e_{nm} . The coefficients, e_n and e_{nm} , are defined as ratios of the rebound to incident normal velocity at the contact point and the mass center, respectively. Figure 8 shows the simulation results for the fixed initial normal velocity and fixed orientation angles (the incident velocity is 2 m/s; the orientation angles are 20° and 45°). The length ratio, ρ_r , changes from 0 to 50 with an increment of 0.5. For a microsphere, $\rho_r = 0$. The microbody is called long and slim when $\rho_r > 10$. As ρ_r increases, its effect on e_n becomes weaker. No significant change in e_n is observed when $\rho_r > 10$. Because the total energy dissipation happens locally at the contact area near the spherical tip according to the current simulation model, the energy dissipation does not change as ρ_r varies. When ρ_r is small, less kinetic energy is converted into rotational energy. Thus the percentage of energy dissipation through rolling and sliding is smaller.

The model also predicts a higher e_n for small ρ_r . The frictional energy dissipation increases when ρ_r increases. However, when ρ_r is very large, the total kinetic energy that is converted

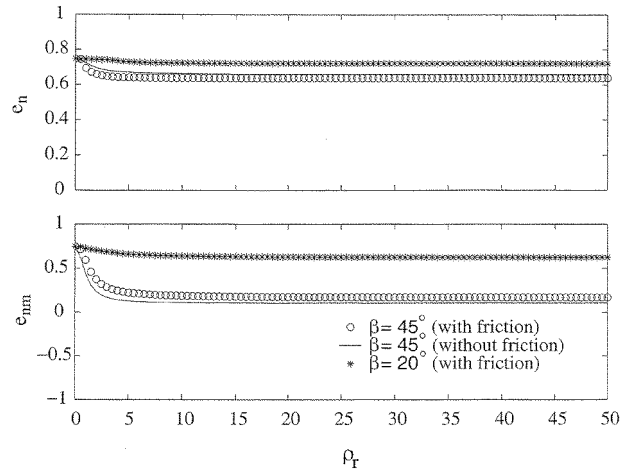


Figure 8. The coefficients of restitution versus the length ratio for 2 hemispheres connected by a rigid rod with no mass ($\beta = 45^\circ$ and 20°).

into rotational energy reaches a practical limit. Thus for very long and slim microbodies, the increase in length does not make much difference on e_n and the change in e_n becomes more negligible. The effects of friction can also be observed in Figure 8. The change in friction coefficient from $f = 0.0$ to $f = 0.15$ slightly decreases the rebound velocity at the contact tip but increases the rebound velocity at the mass center. This is caused by the increase of rotation due to friction during impact. For a slim microbody ($\rho_r > 1.0$), the mass center rebound velocity is always smaller than the contact tip rebound velocity ($e_n > e_{nm}$). Thus the microbody rotates after rebound. If gravity is introduced, the rod is pulled back toward the surface and a second impact will occur at the other end of the microbody.

Cylindrical Rod

In reality, the mass also changes when the shape of the microbody changes. To simplify the analysis, the rod shown in Figure 6 is used in the impact simulation. The shape of the rod is determined by the radius of the cross section, r_0 , and the distance between the center of the spherical ends, L . The length ratio, ρ_r , is still defined as the ratio of length to radius, $\rho_r = L/r_0$. Figure 9 shows the simulation results. As ρ_r increases, e_n increases. This result can be explained by damping. In the current model, energy is dissipated locally at the contact area and ζ_A and ζ_H are held fixed. According to Equations (4) and (5), both Hertzian and adhesion damping are independent of the length ratio. Thus the energy dissipation per unit mass is proportional to $1/m$. When mass increases, the energy dissipation per unit mass decreases. Lower energy dissipation per unit mass gives a higher coefficient of restitution, e_n . However, the increasing rate of e_n decreases for longer rods because when the mass increases, the ratio of energy dissipation to the total kinetic energy becomes smaller. As a limit, the energy dissipation ratio is zero for a rod with infinite length and infinite kinetic energy. Therefore the

limit for e_n is unity, which happens when the rod is infinitely long and $\rho_r = \infty$. From Figure 9, it is clear that the effects of friction are similar to the cases shown in Figure 8. Friction decreases e_n slightly but increases e_{nm} , and its effects on the mass center velocity are larger than the contact tip. The increase in orientation angle decreases e_n slightly and e_{nm} significantly. For the case of $\beta = 20^\circ$, when $\rho_r < 2$, e_n increases because of the increase of the total mass. When $\rho_r > 2$ the increase of the rotational energy dissipation overcomes the effects of mass and e_{nm} begins to decrease. Comparison of the $\beta = 45^\circ$ case shows that the increase period for e_{nm} is shorter for larger orientation angles (which corresponds to the shallow angle oblique impact). The effect of the length is more significant for larger orientation angles. In the case of $\beta = 45^\circ$, e_{nm} is negative when $\rho_r > 5$. However, the corresponding e_n is always positive. A negative value of e_{nm} indicates that the normal velocity of the mass center of the rod does not reverse as the contact tip rebounds. This implies that a second impact can occur after the end of the first impact.

Simulations for the same rod are conducted in which the initial orientation angle is varied to further understand the effects of the initial orientation angle. The results are shown in Figure 10. The initial conditions for all the cases in Figure 10 are as follows: $\alpha = \gamma = 0^\circ$, $v_t = v_t' = 0$ m/s, $v_n = 5$ m/s, and $\beta = 0^\circ$ to 90° . Note that for angles approaching 90° , the contact area may no longer be circular. Although the initial tangential velocity components are zero, because of the orientation angle rotation is generated during impact. The initial orientation of the rod affects the normal velocity at the contact area. The normal velocity caused by rotation also affects the rebound velocity. Figure 10 shows that for constant dissipation parameters at the contact area, the value of the restitution coefficient at the contact point drops when the initial orientation angle increases ($\beta = 0^\circ$ corresponds to the normal orientation) if $\rho_r > 0$. The case of $\rho_r = 0$ corresponds to the sphere impact. The coefficient

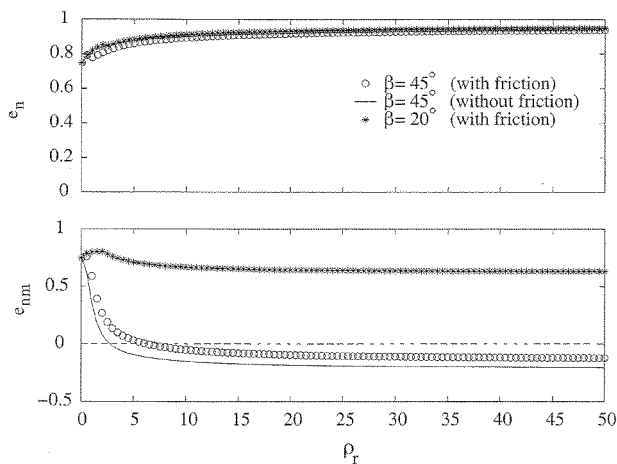


Figure 9. The coefficients of restitution versus the length ratio for a rod with 2 spherical ends ($\beta = 45^\circ$ and 20°).

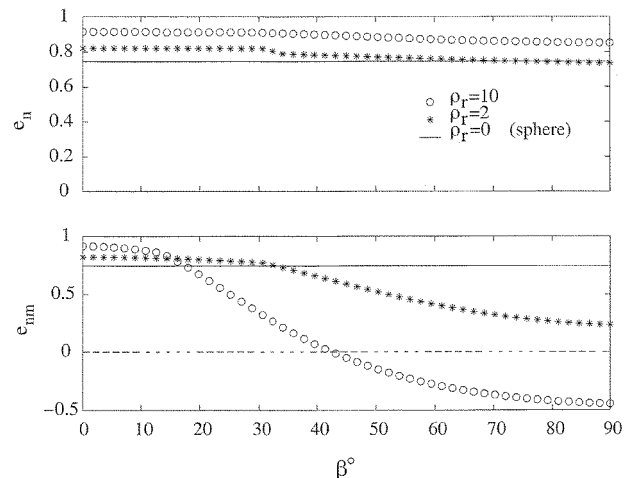


Figure 10. The coefficients of restitution versus the incident angle for a rod with 2 spherical ends ($\rho_r = 10, 2$, and 0).

of restitution for the sphere impact is independent of the orientation angle. At normal orientation the mass center and the contact tip have the same rebound velocities because there is no rotation and friction is not generated. As β increases (the orientation becomes more oblique), the coefficient of restitution at the mass center decreases significantly. The rate of decrease is higher for larger length ratio ρ_r . When the rod is long, e_{nm} is negative if the initial orientation angle is larger than a certain value. For the case of $\rho_r = 10$, $e_{nm} < 0$ if $\beta > 42^\circ$. However, the corresponding e_n is still positive. A second impact is likely to occur after the first impact. If the second contact happens, the microbody will likely be captured by the surface after repeated contacts. Thus unlike the sphere impact, the orientation of the rod also affects the “capture.” According to the above simulation results, the “capture” of the microbody is determined by the material properties, the incident velocity, the shape of the microbody, and the initial orientation angles.

The velocities of the mass center of the rod and the contact area during the contact are also plotted to show the effects of friction and rotation. For spheres, the contact time is closely related to the combined material stiffness, K , and the adhesion line force, f_0 . However, the contact time for rod impact as shown in Figures 11 and 13 is also determined by the initial orientation angle, β . With an increase in orientation angle, the contact time decreases. The rebound tangential velocities increase when the angles increase. However, the larger the angle is, the lower the rebound normal velocity is at the mass center. When the orientation angle is larger than a certain value, the rebound normal velocity at the mass center is zero or negative (keeping the same direction after impact). But from Figures 12 and 14, the normal rebound contact velocity at the end of the rod is not significantly affected by the orientation angles. This means that a second con-

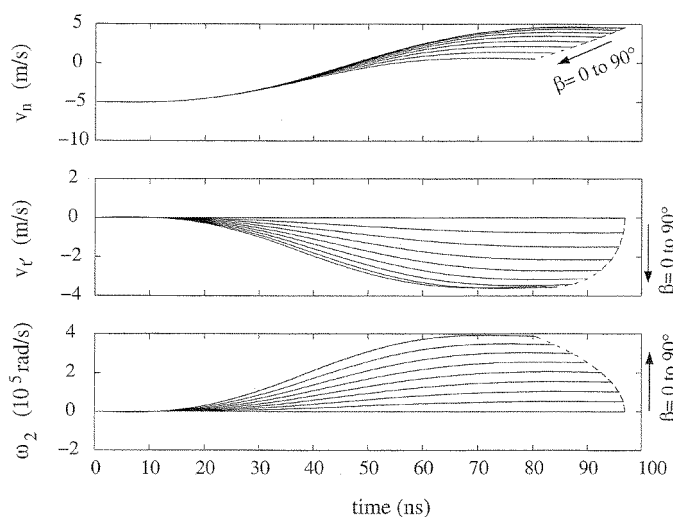


Figure 11. The mass center velocities versus time for rods with different initial orientation angles ($f = 0.7$, $\rho_r = 10$, $v_t = v_{t'} = 0$ m/s, $v_n = 5$ m/s, $\alpha = \gamma = 0^\circ$, and $\beta = 0^\circ$ to 90° , increment = 1°).

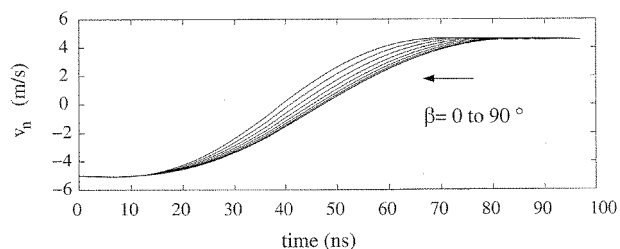


Figure 12. The normal velocity component at the contact tip versus time for rods with different initial orientation angles ($f = 0.7$, $\rho_r = 10$, $v_t = v_{t'} = 0$ m/s, $v_n = 5$ m/s, $\alpha = \gamma = 0^\circ$, and $\beta = 0^\circ$ to 90° , increment = 1°).

tact after the first contact is likely to occur at the other end of the rod if the incident angle is larger than a certain value.

The effects of friction can be observed. Typically, the Coloumb friction coefficient is from 0.1 to 0.7. Figures 12 and 14 correspond to cases when the friction coefficient is 0.7 and 0.15, respectively. For a large friction coefficient, more resistance to tangential motion is placed at the contact area. The tangential velocity at the contact area is relatively very small and the mass center tangential velocity is proportional to the rotational velocity (Figure 11). On the other hand, when the friction coefficient is small, the resistance at the contact area is smaller. The free-end condition applies. The tangential velocity at the contact area is larger (Figure 14). The mass center tangential velocity no longer is proportional to the rotational velocity. However, the tangential motion at the mass center and the contact area in Figure 14 changes directions during contact. In order to identify the reason for the change in direction of tangential motion during impact, the corresponding normal forces during contact are shown in Figure 15. The inversion of the tangential and

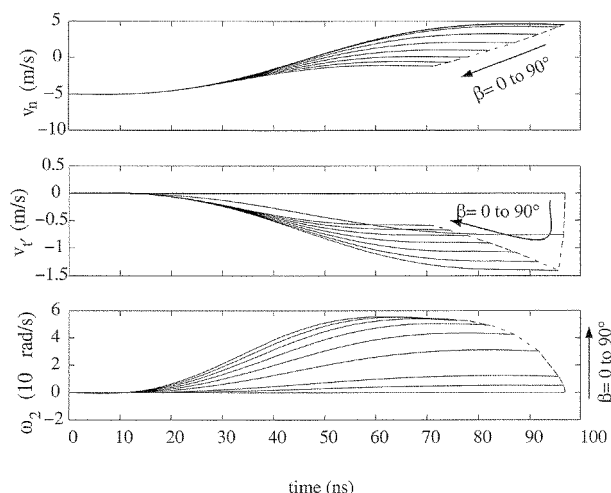


Figure 13. The mass center velocities versus time for rods with different initial orientation angles ($f = 0.15$, $\rho_r = 10$, $v_t = v_{t'} = 0$ m/s, $v_n = 5$ m/s, $\alpha = \gamma = 0^\circ$, and $\beta = 0^\circ$ to 90° , increment = 1°).

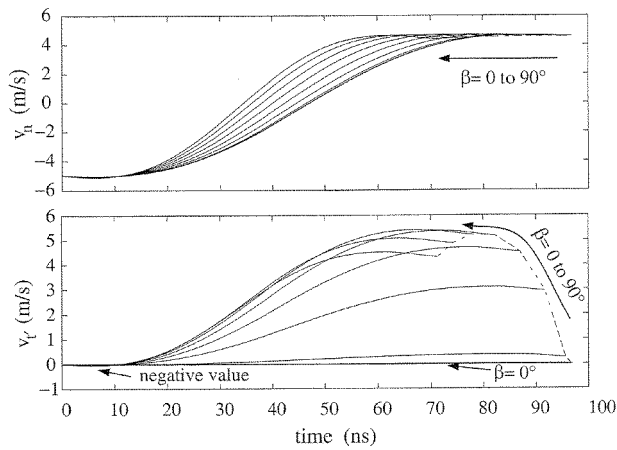


Figure 14. The velocities at the contact tip versus time for rods with different initial orientation angles ($f = 0.15$, $\rho_r = 10$, $v_t = v_t' = 0$ m/s, $v_n = 5$ m/s, $\alpha = \gamma = 0^\circ$, and $\beta = 0^\circ$ to 90° , increment = 1°).

rotational motions occurs when adhesion and damping occurs. At the beginning of the contact in Figure 14, the rod rotates toward the direction that decreases the orientation angle of the rod. After a certain period of time, the rotation and tangential motions change to the opposite direction. Figure 15 shows the normal contact force for the same cases shown in Figure 14. The inverted rotation for large values of β is caused by the change of sign of the normal force and tangential force during contact. Due to adhesion attraction, at the beginning and the end of contact the normal force is negative (along the approaching direction). Between the beginning and the end of contact, the normal force is positive (along the rebound direction). When β is not zero the moment of the normal force about the mass center of the rod changes direction and the inversion of rotation is produced.

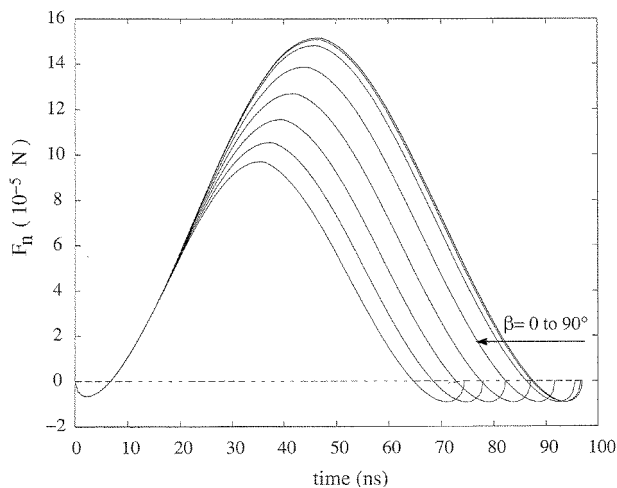


Figure 15. The normal forces during contact for the cases shown in Figure 14.

The model is capable of the simulation of more complicated impacts in which arbitrary initial rotational and translational velocities can be placed about all the principal axes and more complicated microbody geometries can be considered. However, because of the difficulty in understanding the meaning of the simulation results, this paper has only presented several simplified cases to elucidate the potential effects caused by the geometry of the microbody.

CONCLUSIONS

From the simulation results, the following can be concluded.

1. The shape and aspect ratio of the microbody significantly affects the impact response. With the same material, target surface, mass, and curvature radius at the contact tip, when the initial orientation angle is not normal, the impact of a slim body is clearly different from the impact of a sphere. More rotation is generated when the ratio ρ_r increases. Therefore rotational energy balance plays a more important role for slim microbody impacts. The coefficient of restitution at the contact tip for a microbody with $\rho_r > 1.0$ is smaller than that of a sphere. Thus a microbody with $\rho_r > 1.0$ is more likely to be captured by the surface.

2. If the mass of the microbody also changes when ρ_r changes, the coefficient of restitution increases when the mass increases. However, the coefficient of restitution at the mass center decreases to negative values for large orientation angles. Considering the effects of the mass, slim microbodies are captured readily by the surface through secondary and more-multiple impacts.

3. For a given body shape, the impact is also affected by the initial orientation. The orientation angle not only causes different rebound velocities but also influences the possibility of a second impact. If the incident angle is larger than a critical value, the coefficient of restitution at the mass center drops to a negative value. Multiple impacts occur and, due to the resultant energy dissipation and the microbody, is captured by the surface. This is different from the case of the sphere. Thus in the case of the arbitrarily-shaped body impact, surface capture is determined not only by the material parameters but also by the initial conditions.

4. Friction is important in microbody impacts in that it can change the velocity in the tangential direction at the contact tip. When friction is large, the final tangential velocity at the contact tip is zero and the tangential velocity at the mass center is the cross product of the rotational velocity and the positional vector of the mass center. When friction is small, sliding continues through the contact duration. So friction and its moment about the mass center affect the tangential and rotational velocities. The tangential velocity at the mass center is not proportional to the rotational velocity for the small-friction cases when sliding occurs over the contact area.

5. Negative normal loads due to adhesion can cause reverse tangential motions at the contact area.

6. No experimental data are available to verify the simulation results for 3D arbitrarily-shaped microbody impact in the current

stage. However, the simulation for 2D sphere impacts is verified by the experimental data. The simulation results for the impacts between a flat surface and 2 hemispheres connected by a rigid bar with no mass and a rod with 2 hemispherical ends show the importance of geometry and orientation on microbody impacts.

REFERENCES

- Ando, Y., Ishikawa, Y., and Kitahara, T. (1995). Friction Characteristics and Adhesion Force under Low Normal Load, *Transactions of the ASME J. of Tribology* 117:569-574.
- Bowen, R. C., DeMejo, L. P., and Rimai, D. S. (1995). A Method of Determining the Contact Area Between a Particle and Substrate Using Scanning Electron Microscopy, *J. Adhesion* 51:191-199.
- Brach, R. M., and Dunn, P. F. (1995). Macrodynamics of Microparticles, *Aerosol Sci. Technol.* 23:51-71.
- Brach, R. M., and Dunn, P. F. (1996). *Simulation of Microparticle Impact with Adhesion*, Proc. of Adhesion Soc., Symposium on Particle Adhesion, Myrtle Beach, SC.
- Cheng, W., Brach, R. M., and Dunn, P. F. (2002). 3D Modeling of Microsphere Contact/Impacts with Smooth Flat Surfaces, *Aerosol Sci. Technol.* to be published.
- Dahneke, B. (1975). Further Measurements of the Bouncing of Small Latex Spheres, *J. Colloid Interface Sci.* 51:58-65.
- Derjaguin, B. V., Muller, V. N., and Toporov, Yu. P. (1975). Effect of Contact Deformations on the Adhesion of Particles, *J. Colloid Interface Sci.* 53:314-325.
- Israelachvili, J. N., and Tabor, D. (1972). The Measurement of van der Waals Dispersion Forces in the Range 1.5 to 130 nm, *Proc. R. Soc. Lond. A* 331:19-38.
- Johnson, K. L., Kendall, K., and Roberts, A. D. (1971). Surface Energy and the Contact of Elastic Solid, *Proc. R. Soc. Lond. A* 324:301-313.
- Li, X., Dunn, P. F., and Brach, R. M. (1999). Experimental and Numerical Studies on the Normal Impact of Microspheres with Surfaces, *J. Aerosol Sci* 30:439-449.
- Skinner, J., and Gane, N. (1972). Sliding Friction under Negative Load, *J. Phys. D.* 5:2087-2094.
- Tsai, C. J., Pui, D. Y. H., and Liu, B. Y. H. (1991). Elastic Flattening and Particle Adhesion, *Aerosol Sci. Technol.* 15:239-255.
- Wall, S., John, W., Wang, H. C., and Goren, S. L. (1990). Measurements of Kinetic Energy Loss for Particles Impacting Surfaces, *Aerosol Sci. Technol.* 12:926-946.
- Xu, M. D., and Willeke, K. (1993). Right-Angle Impaction and Rebound of Particles, *J. Aerosol Sci.* 24:19-30.